JOURNAL OF OPTOELECTRONICS AND ADVANCED MATERIALS, Vol. 11, No. 5, May 2009, p. 583 - 589

Results on nanosized $CaTiO_3:Pr^{3+}$ phosphor

C. GHEORGHIES*, P. BOUTINAUD[a], M. LOÏC[a], VALERIU O. ATANASIU[b]
Dunarea de Jos University of Galati, Faculty of Science, str. Domneasca no.47, Romania
[a]Blaise-Pascal University, Ecole Nationale Supérieure de Chimie de Clermont-Ferrand, Ensemble Scientifique des Cézeaux - B.P. 187-63174 Aubière Cedex , France
[b]Dunarea Secondary School, Galati, Romania

Luminescent films of $Pr3^+$-doped Ca TiO_3, being superior to those of the type $Y_2O_3:Eu^{3+}$, have been prepared by sol-gel (S-G), dip-coating (D-C), radio-frequency sputtering (R-FS) and spray (S) technologies. The structure, microstructure and chemical composition of these films were characterized by XDR, AFM, electron microscopy and Rutherford Back Scattering (RBS). The response of these films under UV pumping was estimated by time-resolved laser spectrometry (T-RLS). The irradiative transition and photoluminescence performances of films strongly depend on sintering conditions or applied thermal treatment, that affect both the structural and microstructural characteristics. The photoluminescence intensity increases along with growing of the sintering temperature, whilst the brightness increases for D-C films and decreases for films prepared by (S) technique.

Received March 2, 2009; accepted May 25, 2009)

Keywords: $CaTiO_3:Pr^{3+}$ Phosphor**,** Structure, Photoluminescence spectra

1. State of the art

Nowadays, luminescent materials (otherwise called phosphors) are more and more present in every day's life. Apart from traditional and historical applications in lighting (fluorescent lamps), screens (cathodic ray tubes, plasma display panels), solid state lasers ($Al_2O_3:Cr^{3+}$, YAG:Nd^{3+}, etc.), optical communication (Er^{3+}-doped fibers), optoelectronics or sensors, they find more and more applications in new technical fields like marine and aeronautical navigation [1, 2], nuclear medicine (bioluminescence and immunology) [3], archaeology [4], environment (ozone analyzers, nitrogen oxides, sulphur compounds or toxic particles), [5, 6], energetic (monitoring the combustion processes in power stations and at the intern combustion engines) [7], and also bioinformatics, biophysics, biochemistry, quantum chemistry or digital television, etc. [8, 9].

In spite of very active researches on phosphors for more than 50 years all over the world, the lighting, display and optoelectronics industries still face the challenge of using more durable, energy-efficient, cost-effective and environmentally safe phosphors to meet their increasingly creative applications in everyday devices, such as TV screens, mercury free and energy saving lighting, electronic billboards, computer monitors, portable electronics etc. Owing to this challenge, breakthroughs are expected from the development of new preparation methods (especially soft chemistry routes) for obtaining nanocrystals, fibers, functional hybrid materials or nanostructured films. The Pr^{3+}-doped perovskite phosphor $CaTiO_3:Pr^{3+}$ is of special interest, both from fundamental and applicative viewpoints [10-12].

2. Fundamental aspects on luminescence properties of $CaTiO_3:Pr^{3+}$

The perovskite structure is named after the mineral $CaTiO_3$. At room temperature, the structure is orthorhombic and is made up of corner shared TiO_6 octahedra with Ca ions in the large cavities at the corners of the unit cell, as depicted in figure 1. The Pr^{3+} ions are expected to occupy the C_{1h} calcium sites. This situation results in the presence of 2 very short Pr^{3+} - Ti^{4+} interatomic distances of 3.17 Å, which makes possible a photon assisted energy transfer from Pr^{3+} to Ti^{4+} at relatively low energy. This energy transfer, referred to as Pr^{3+} / Ti^{4+} ↔ Pr^{4+} / Ti^{3+} Inter Valence Charge Transfer (IVCT) has been proved to interfere strongly with the excited dynamics of the Pr^{3+} ion in $CaTiO_3:Pr^{3+}$, thus causing the quenching of the otherwise prominent greenish-blue emission from the $^3P_0$ level ($^3P_0 \rightarrow {}^3H_4$ transition, see the energy level structure of Pr^{3+} shown in figure 2, where the level $^1S_0$ is not shown) [14, 15]. Consequently, only a single emission from the $^1D_2$ level is observed in the visible ($^1D_2 \rightarrow {}^3H_4$ transition), giving a pure red saturated color to the luminescence of $CaTiO_3:Pr^{3+}$, with chromaticity coordinates x = 0.68 and y = 0.31 (see figure 3, where the color point of $CaTiO_3:Pr^{3+}$ is indicated as the white circle), very close to those of the "ideal" red, as defined by the International Commission on Illumination [17]. The quenching process of the $^3P_0$ emission by IVCT is detailed in figure 4, where the configurationally coordinate diagrams show the position effect of the IVCT on the population of the $^3P_0$ and $^1D_2$ emitting states.

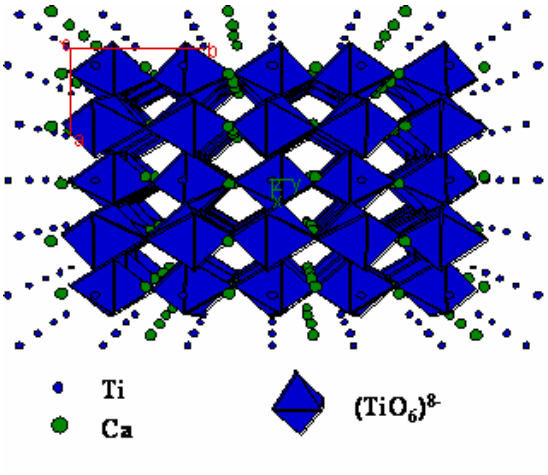

Fig.1. The perovskite structure of $CaTiO_3$

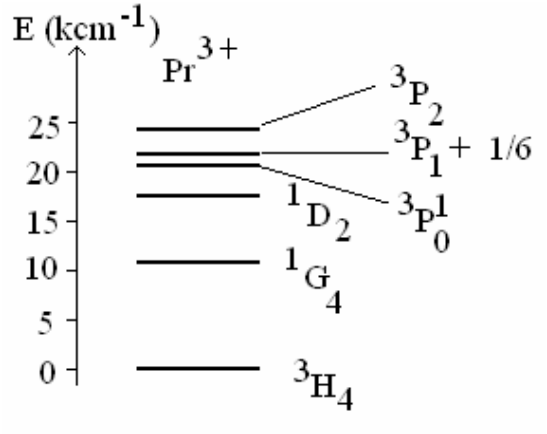

Fig.2. The energy-level structure of Pr^{3+}

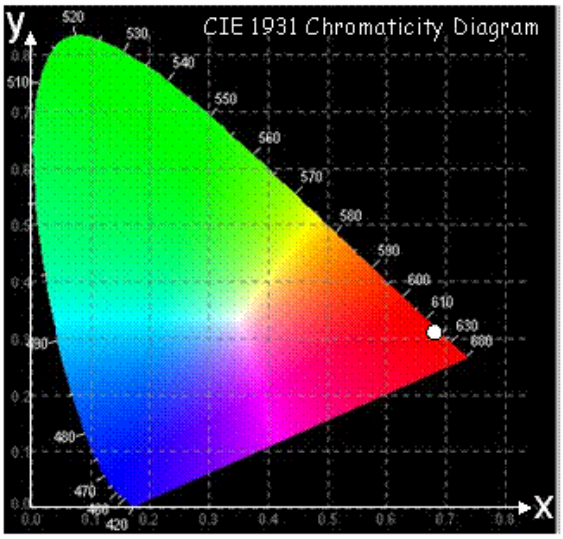

Fig. 3. CIE diagram.

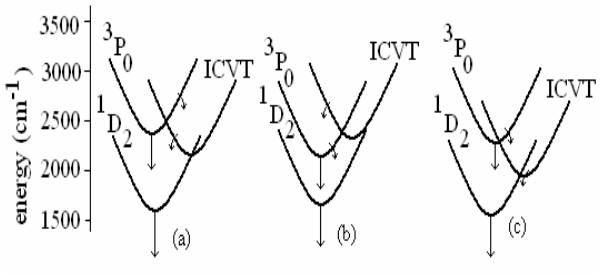

Fig. 4. Configurationally coordinate diagram: the effect the position of the IVCT

Interestingly, the quenching of the $^3P_0$ emission of Pr^{3+} by IVCT has been demonstrated to be a general behavior in a number of oxidizing host lattices containing d^0 closed shell transition metals like titanates, vanadates, niobates, tantalates, etc.[18].

The graph plotted in figure 5 shows the relationship existing between the IVCT energy, the optical electronegativity χ_{opt} (M^{n+}) of the transition metal ion (i. e. its aptitude to electron capture) and the shortest Pr^{3+} - transition metal distance in the lattice d(Pr^{3+} - M_{n+}). This behavior is rationalized in an equation of the form:

$$IVCT(\mathrm{Pr}^{3+}, cm^{-1}) = 58800 - 49800\frac{\chi_{opt}\left(M^{n+}\right)}{d(\mathrm{Pr}^{3+} - M^{n+})}$$

Although it is empirical, this equation can be used as a predictive tool to prepare red emitting oxides- based compounds doped with small amounts Pr^{3+}. In particular, it has been demonstrated that compounds having IVCT energy lower than 28,000 cm^{-1} emit single red luminescence only from the $^1D_2$ level, like for instance $YVO_4:Pr^{3+}$ or $LiNbO_3:Pr^{3+}$ [18]. More recently, this approach has been extended to the case of Tb^{3+} ions that possess a relatively low fourth ionization potential (i. e. an aptitude to oxidization), similarly to Pr^{3+}.

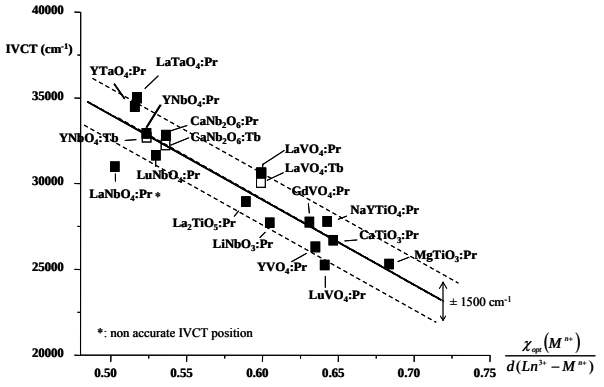

Fig. 5. Variation of the IVCT band position against the ratio between the optical electronegativity of the closed-shell transition metal cation (M^{n+}) and the shortest interatomic distance between Ln^{3+} (Ln = Pr, Tb) and M^{n+}.

3. Experimental results on structure and luminescence properties of $CaTiO_3:Pr^{3+}$

The red phosphor $CaTiO_3:Pr^{3+}$ is an exceptional compound regarding to its applicability in a number of different technological fields. This phosphor was firstly studied in the beginning of the 1990 and is a very promising material for low voltage field emission display (i. e. for flat cathode ray screens) [19]. Up to now, the commercial red phosphor that is used in plasma display panels (PDPs) is $Y_2O_3:Eu^{3+}$. This phosphor is extremely bright due to the extremely sharp hypersensitive $^5D_0 \rightarrow {}^7F_2$ electronic transition (this phosphor is the brightest ever prepared for the red spectral range) However, although this phosphor is well adapted to mercury excitation at 254 nm, it is not optimized for a VUV xenon-neon plasma excitation. In addition, its luminescence is not purely red but reddish-orange due to some luminescence contributions (viz. $^5D_0 \rightarrow {}^7F_1$ and $^5D_0 \rightarrow {}^7F_0$) at shorter wavelength compared to $^5D_0 \rightarrow {}^7F_2$. Lastly $Y_2O_3:Eu^{3+}$ is a relatively expansive phosphor and represents about a quarter of the total price of a flat plasma display screen. Actually, $CaTiO_3:Pr^{3+}$ is much cheaper than $Y_2O_3:Eu^{3+}$: the only rare earth present in Pr^{3+} and this is the cheaper among all the rare earths; moreover, the optimized doping rate in $CaTiO_3:Pr^{3+}$ is only 0.1 mol% Pr^{3+} whereas it is higher than 5% Eu^{3+} in $Y_2O_3:Eu^{3+}$. In addition, as mentioned above, the color of the red emission in $CaTiO_3:Pr^{3+}$ is almost the ideal one, which avoids using filters to improve the color rendering. Lastly, it is has to be noticed that the excitation spectrum of $CaTiO_3:Pr^{3+}$ is very broad and approximately flat (see figure 6) from the near UV to the VUV (i. e. 150 nm and even below – not shown here). Especially, such an excitation profile is suitable for efficient excitation using VUV Neon/Xenon plasma and allows considering $CaTiO_3:Pr^{3+}$ as a potentially attractive phosphor for PDPs.

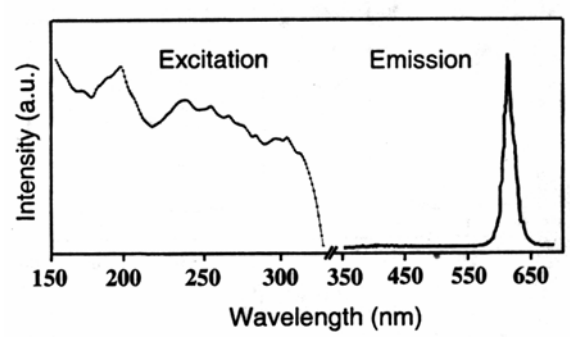

Fig.6. Typical excitation-emission profiles of $CaTiO_3:Pr^{3+}$ at 300 K

It is also worthwhile noting that the behavior described above for $CaTiO_3:Pr^{3+}$ is of special interest for the design of new powder phosphors usable in mercury-free lamps. It is well-known that fluorescent lamps (also called fluocompact lamps) present the great advantage over incandescent lamps to glow the same amount of visible light for a much lower consumed electrical power (the yield is 14-25 lumens/watt for incandescent lamps and 60-70 lumens/watt for fluocompact lamps) and to have a lifetime 6 to 15 times longer. The principal drawback of these mercury - based fluorescent lamps (apart form the price) is linked with the management of the end of their lives. Indeed, the amount of undesirable mercury vapor which is freed in our environment every year in the world from the wasted lamps is close to 5 tons.

In addition to the above properties, $CaTiO_3:Pr^{3+}$ has also been experienced recently as a red afterglowing phosphor. An afterglowing phosphor shows the advantage to keep emitting light after light irradiation has stopped. There is a real commercial need for red-emitting long lasting phosphors for technological applications in dark vision displays emergency route marking, warning sign boards, sensing of structural damage and fracture of materials, etc. [20- 22]. Up to now, long lasting phosphorescences have been reached in the blue and the green spectral ranges by incorporating Eu^{2+} and Dy^{3+} ions in strontium and calcium aluminates. For the red component, the afterglowing phosphors are still limited to sulfides like $CaS:Eu^{3+}$ or $SrS:Eu^{3+}$, with the problem that sulfides sometimes show chemical instabilities, depending on the applications [23, 24]. This knowledge is now used to improve the long lasting afterglow in this phosphor. In particular, it was demonstrated the possibility of observing afterglow not only after UV irradiation but also after blue irradiation in the blue spectral range. The afterglow emission spectra of $CaTiO_3:Pr^{3+}$ at room temperature after one minute irradiation at 330 nm (valence-to-conduction band transition), 380 nm (IVCT) or 450 nm (intraionic $^3H_4 \rightarrow {}^3P_2$ transition) in figure 7 is showing. The scale is the same for all spectra. These spectra cover the first 30 seconds of afterglow. A time delay of 2 seconds separates each spectrum.

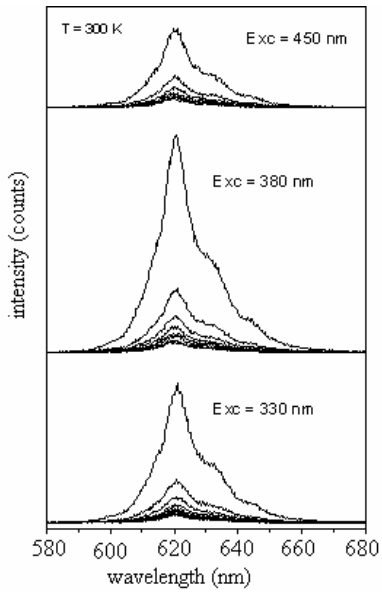

Fig. 7.The afterglow emission spectra of $CaTiO_3:Pr^{3+}$ at room temperature after one minute irradiation at 330 nm.

The sol-gel technology is a very powerful method for preparing inorganic polycrystalline compounds with controlled grain sizes, morphologies and textures either in the micrometer or in the nanometer scale (figure 8). This technology is also very useful for the deposition of films and was used to deposit $CaTiO_3:Pr^{3+}$ either by spin coating, dip coating, spray pyrolysis or radio-frequency sputtering.

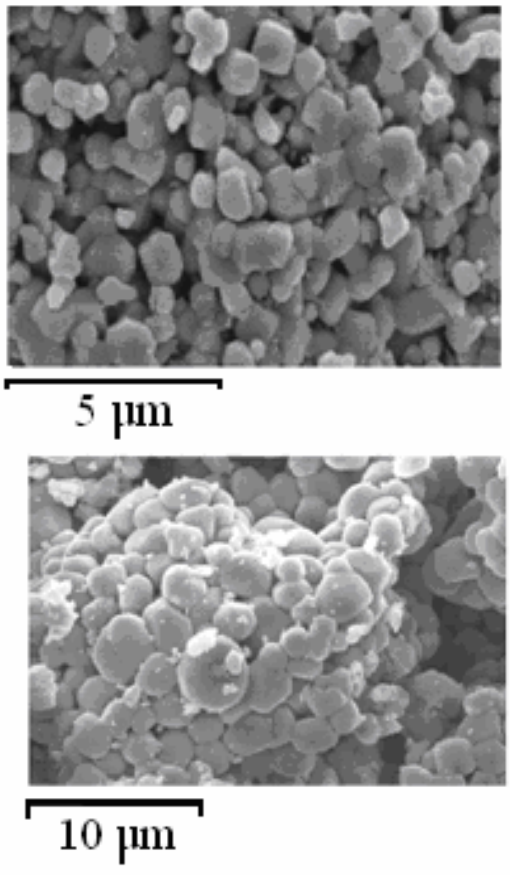

Fig. 8. Scanning electron micrographs of a $CaTiO_3:Pr^{3+}$ powders

High quality photoluminescent coatings of $CaTiO_3:Pr^{3+}$ were obtained by the above mentioned methods. The thicknesses of the films varied from ≈ 200 nm (spin coating, dip-coating and sputtering) to several micrometers (spray pyrolysis). In every case, special care was taken to control the *in situ* crystallization of the as-deposited films by temperature dependant X-ray diffraction measurements [25]. Figure 9 shows typical patterns recorded for sprayed films. It is interesting to observe in this case the beginning of crystallization of the $CaTiO_3$ perovskite at about 550 °C, against more than 1000 °C for the same perovskite prepared by conventional solid state methods. The average size of the crystallites for the spray films heated at 1000°C was estimated at about 75 nm using Scherrer's equation.

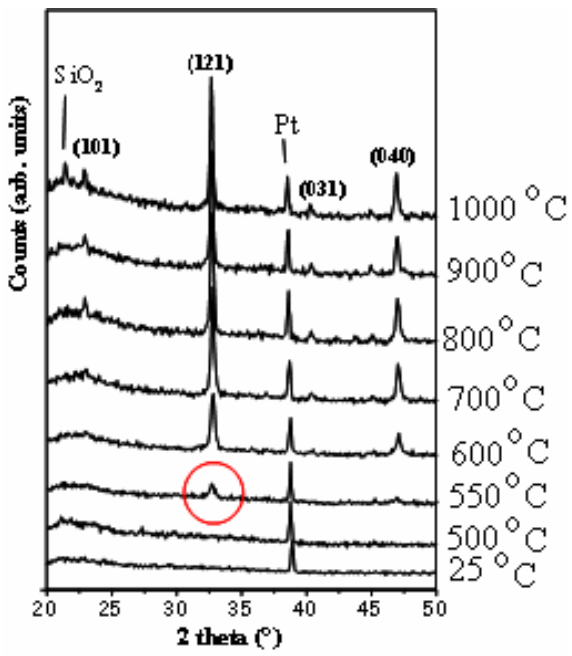

Fig.9. X-ray diffraction patterns of a $CaTiO_3:Pr^{3+}$ film deposited by spray.

After heat treatment, the films were more or less translucent, depending on the amount of deposited matter. The surface aspect changed drastically with the temperature of thermal treatment as shown in figure 10. The film heated at 800°C presents a step-like structure with ladders piling up perpendicularly to the substrate, but after being heated at 1000°C, the surface became uniformly smooth and presented a very good adherence, as in the case of phosphor penetration within the substrate.

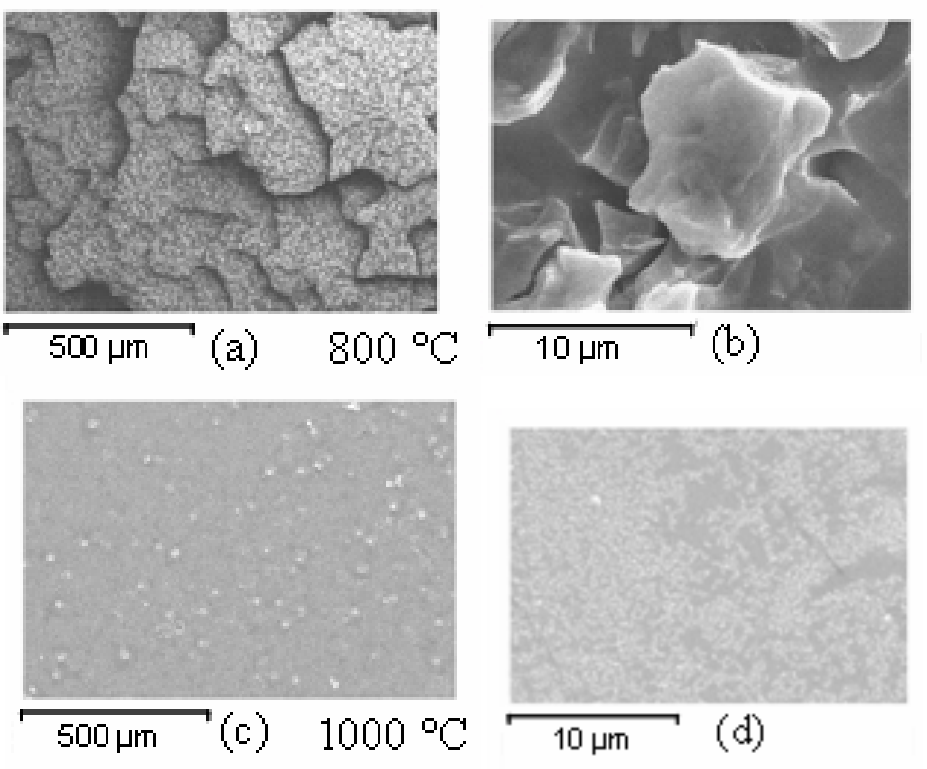

Fig. 10. Scanning electron micrographs of a $CaTiO_3:Pr^{3+}$

The photoluminescence of sprayed coatings, with different thicknesses, under natural light (a) and 254 nm light (b) is relatively bright, as shown by fig. 11.

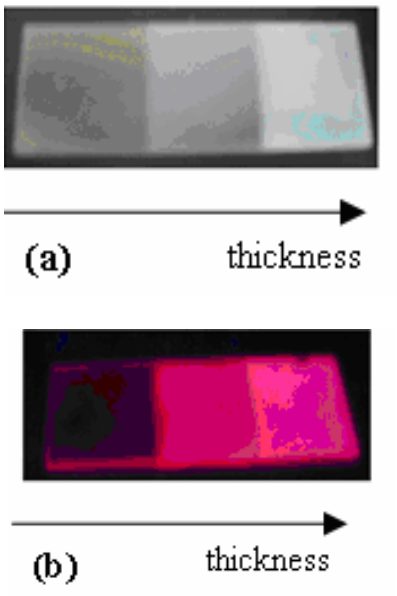

Fig. 11 Sprayed coatings of $CaTiO_3:Pr^{3+}$

The photoluminescence in dip-coated or sputtered films is much weaker relative to sprayed films, due to their much lower thicknesses. Nevertheless, the red luminescence is still observable by naked eye. Detailed photoluminescence measurements performed by time-resolved laser spectroscopy allowed us to conclude about the high level of crystallization of all the films, using for this purpose the Pr^{3+} luminescence as a local structural probe. This is particularly evident from figures 12 and 13 where it is possible to observe the characteristic Stark level structure of both $^1D_2$ excited state and $^3H_4$ ground state of the Pr^{3+} ions located in well defined single sites in the perovskite structure. The spectra of a powder heated at 1000°C and having the same composition as films are given for comparison purposes.

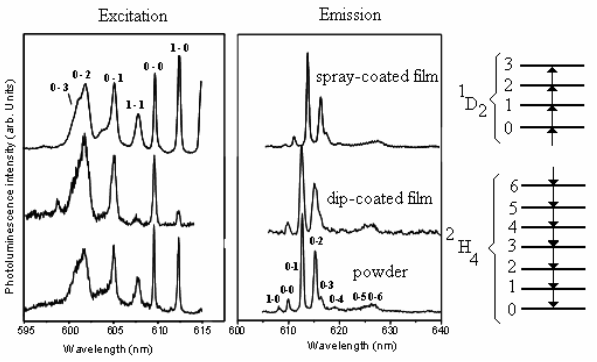

Fig. 12. Photoluminescence spectra at 15K of $CaTiO_3:Pr^{3+}$ films deposited by soft routes.

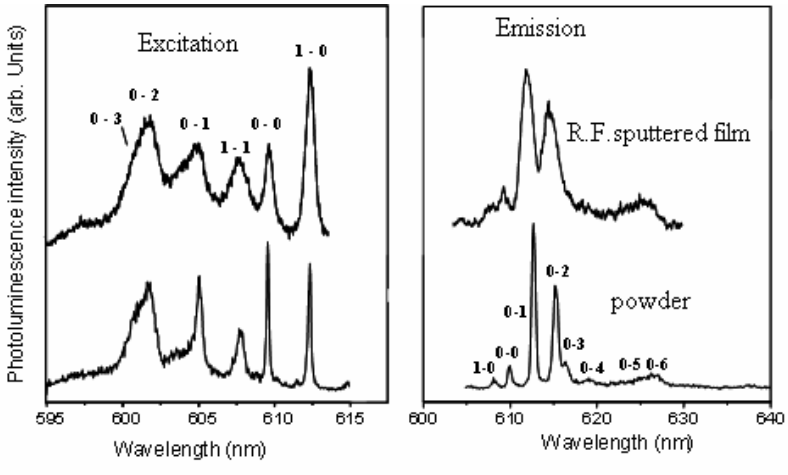

Fig. 13. Photoluminescence spectra at 15K of $CaTiO_3$:Pr^{3+} films deposited by RFS

In the case of films deposited by R-FS, it is interesting to note a broadening of the electronic transitions relative to the powder of same composition (see figure 13), denoting a nanosized effect. This nanosized distribution of grains in those films was further confirmed by AFM the tapping mode, as represented in figure 14. In addition, the chemical composition of the films was confirmed by RBS measurements (figure 15) of films under various sputtering conditions. A: working pressure 1.5 Pa and Ar / (Ar + O_2) = 100%, B: working power 16.73 W.cm^{-2} and Ar / (Ar + O_2) = 100%, C: working power 16.73 W.cm^{-2} and working pressure 1.5 Pa. Their overall optical quality was evidenced by the interference fringes observed in UV-visible transmission spectrometry (Fig. 16).

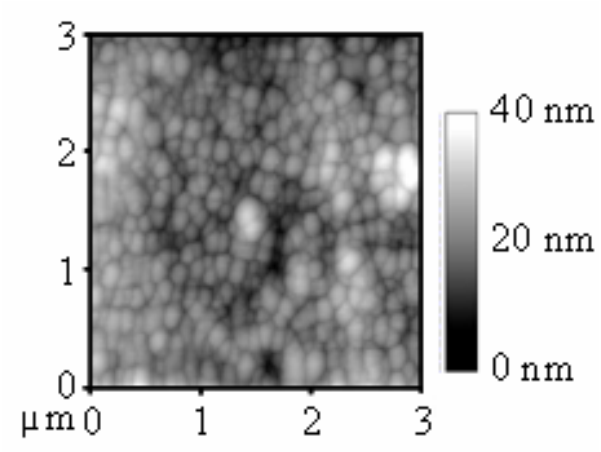

Fig. 14. AFM images of a film of $CaTiO_3$:Pr^{3+} deposited by R- FS and annealed at 800°C

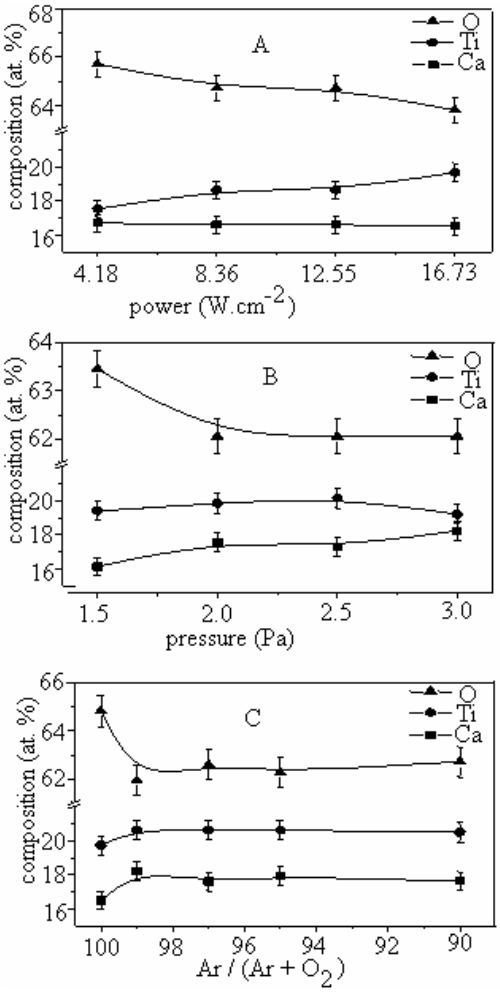

Fig. 15. RBS analysis of the atomic composition of deposited films

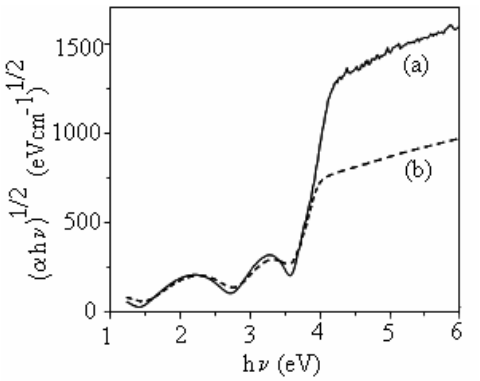

Fig. 16. UV-visible transmission spectra of a film of $CaTiO_3:Pr^{3+}$ deposited by R-FS and annealed at 800°C (a) and at 1000°C (b).

The observation of interferences in the visible - near UV part of the transmission spectra where the absorption is low (i. e. $\lambda > \approx 345$ nm) made it possible the evaluation of the refraction indexes and the thickness of the films using the Swanepöel procedure [26]. Average values of the refraction index at $\lambda = 632.8$ nm range typically from 2.08 in films heated at 700°C to 2.25 in films heated at 800 and 900 °C. The index value decreases to 2.12 for thin films heated at 1000°C. These values are systematically ≈ 10 % lower than in $CaTiO_3$ bulk. The thickness of the films was evaluated close to 200 ±10 nm and did not vary significantly with the temperature of thermal treatment or the sputtering conditions.

4. Conclusions

Luminescent films of Ca TiO_3: Pr^{3+} have been prepared by various techniques including: sol-gel, dip-coating, radio frequency sputtering and spay technologies having as substrate silica. The photoluminescence performances of prepared films are strongly influenced of preparation conditions, the possibly applied thermal treatments them influencing both crystalline structure and/ or microstructure. The photoluminescence of prepared films has been excited by using an UV pump that lead to a transition between the metastable $^1D_2$ level to the $^3H_4$ ground state of Pr^{+3} ions. The presence of the Stark components can be explained taking in account the fact that the Pr^{+3} ions occupy single well-defined crystallographic site in the orthorhombic structure of Ca TiO_3: Pr^{3+}. Detailed photoluminescence measurements performed by T-RLS allowed us to conclude about the high level of crystallization of all the films, using for this purpose the Pr^{3+} luminescence as a local structural probe.

References

[1] J. Bisquert, Synthesis, Properties, and Applications of Oxide Nanomaterials, John Wiley & Sons, Inc., 2007.
[2] S. O. Flyckt, C. Marmonier, Photomultiplier Tubes: Principles and Applications, Photonis, Brive, France, 2002.
[3] H. Martin, Basic Methods for the Biochemical Lab, Springer, Berlin, 2006.
[4] J.-A. Dickmann, F. Pirson, Wohnen und Arbeiten im antiken Pompeji, Antike Welt **1**, 81 (2002).
[5] M.S. Clark, W. R. Horwath, C., Shennan, K. M. Scow, J. Agron, **90**, 662 (1998).
[6] A. S. Medel, Room temperature phosphorescent detection for optical sensors, 7-th European Conference on Optical Chemical Sensors and Biosensors, Madrid Spain, April, 4-7, 2004.
[7] S. Ekambaram, Solution combustion synthesis and luminescent properties of perovskite red phosphors with higher CRI and greater lumen output, Journal of Alloys and Compounds, **390**(1-2), L7 (2005).
[8] O. N. Jensen, Interpreting the protein language using proteomics, Nat. Rev. Mol. Cell Biol, **7**(6), 391 (2006).
[9] O. N. Jensen, Automated phosphorylation site mapping, Nature Biotechnology - **24**, 1226 (2006).
[10] S. Lemanceau, G. Bertrand-Chadeyron, R. Mahiou, M. El-Ghozzi, J.C. Cousseins, P. Conflant, R. N. Vannier, J. Solid State Chem., **148**, 229 (1999).
[11] A. C. Franville, D. Zambon, R. Mahiou, Y. Troin, Chem. Mater. **12**, 428 (2000).
[12] L. Lou, D. Boyer, G. Bertrand-Chadeyron, E. Bernstein, R. Mahiou, J. Mugnier, Optical Materials, **15**, 1-6 (2000).
[13] P. T. Diallo, K. Jeanlouis, P. Boutinaud, R. Mahiou, J. C. Cousseins, J. Alloys and Comp. **323-324**, 218 (2001).
[14] E. Pinel, P. Boutinaud, R. Mahiou, Journal of Alloys and Compounds, **380**, 202 (2004).
[15] P. Boutinaud, E. Pinel, M. Dubois, A. P. Vink, R. Mahiou, Journal of Luminescence **111**, 69 (2005).
[17] P. T. Diallo, P. Boutinaud, R. Mahiou, J. C. Cousseins, Physica Status Solidi (a), **160**, 255 (1997).
[18] P. Boutinaud, R. Mahiou, E. Cavalli, M. Bettinelli, Journal of Applied Physics, **96** 4923 (2004).
[19] Patent n° DE 19534075 Al "Phosphor und Fluoreszenzanzeigevorrichtung" 1994.
[20] E. Nakazawa, T. Mochida, J. Lumin., **72-74**, 236 (1997).
[21] D. Haranath, A. F. Khan, H. Chander, J. Phys. D: Appl. Phys. **39**, 4956 (2006).
[22] C. N. Xu, T. Watanabe, M. Akiyama, X. G. Zheng, Appl. Phys. Lett. **74**, 2414 (1999).
[23] P. J. Deren, S. Kaczynski, A. Czoppa, R. Pazik, W. Strek, Ph. Boutinaud, R. Mahiou, Journal of Alloys and Compounds, 04.197, 2007.
[24] X. Zhang, J. Zhang, X. Ren X.-J. Wang, J., Solid State Chem., **181**(3), 393 (2008).
[25] C. Gheorghieş, L. Gheorghieş, G. Fetecău, J. Optoelectron. Adv. Mater. **9**(9), 2795 (2007).
[26] R. Swanepöel, J. Phys. E Sci. Instrum., **16**, 1214 (1983).

*Coresponding address: cgheorg@ugal.ro